Effects of competing short- and long-range dispersive interactions on discrete breathers

P. G. Kevrekidis, Yu. B. Gaididei,* A. R. Bishop, and A. Saxena
Theoretical Division and Center for Nonlinear Studies, Los Alamos National Laboratory, MS B262, Los Alamos, New Mexico 87545
(Received 12 May 2001; revised manuscript received 13 July 2001; published 19 November 2001)

The discrete nonlinear Schrödinger equation with competing short-range and long-range interactions is considered in spatial dimensions $d \geqslant 2$. This model equation is derived for a situation of two linearly coupled excitations (independently of dimension), and we analytically and numerically study its properties in $2+1$ dimensions. We analyze theoretically and demonstrate numerically the dependence of the discrete breather solutions on the amplitude and range of the interactions. We find that complete suppression of the existence thresholds obtained recently for short-range interactions can be achieved beyond a critical value of the amplitude or of the range of the long-range kernel. For supercritical values of the corresponding parameters, staggered branches of solutions are obtained both in theory as well as in the numerical experiment.

DOI: 10.1103/PhysRevE.64.066606 PACS number(s): 63.20.Pw

I. INTRODUCTION

Physical systems with interplay between discreteness, dispersion, and nonlinear interactions are abundant in condensed matter physics. Examples include spin dynamics in magnetic crystals [1], nonlinear charge and excitation transport in solids [2] and biological systems [3–6], electromagnetic energy propagation in superlattices [7–10], and photonic crystals [11,12]. As a result of this interplay, new types of nonlinear excitations may appear. They are the intrinsically localized oscillatory states, which are also termed discrete breathers (see, e.g., the review article [13]). Herein the term breather specifically refers to intrinsically localized modes (ILM's) which are spatially exponentially localized and temporally periodic solutions of the pertinent equations. Furthermore, for the purposes of this study, we will restrict ourselves to standing wave solutions of this type. Intrinsically localized states have attracted considerable attention because of their ability to focus energy. In this way they offer a novel mechanism for energy localization, an important issue in many physical and biophysical processes [14] and many fields of materials science [15].

Most attention has been focused on one-dimensional systems. However, there have been some studies of higher-dimensional systems. A rigorous proof of the existence of breathers in higher-dimensional systems was given in [16]. Also, intrinsically localized excitations in a two-dimensional Fermi-Pasta-Ulam model [17,18], a Klein-Gordon equation model [19–21], and a two-dimensional discrete nonlinear Schrödinger (NLS) model [22–25] were investigated. Breathers in a discrete two-dimensional NLS model with dispersive dipole-dipole interactions were studied in [26].

The effects of short-range and long-range dispersive interactions have mostly been investigated separately. By dispersive interaction we mean that the excitation energy acquires a wave-vector dependence. However, there are physical situations where long-range dispersive interations coexist and compete with short-range ones. For example, the DNA molecule contains charged groups, with long-range Coulomb interaction between them. Thus, the corresponding vibrational excitations besides a short-range coupling between base pairs [4] also have a long-range dipole-dipole dispersive interaction [6]. The excitation transfer in quasi-two-dimensional molecular crystals [27] and Langmuir-Blodgett-Scheibe aggregates [28] is due to both short-range quadrupole-quadrupole and long-range dipole-dipole interactions. Depending on molecular orientations these two types of interactions can either compete or reinforce each other. Here we give an example of a system where the dispersion curves of two elementary excitations are close in energy, and effective long-range transfer occurs through the coupling between the excitations.

The paper is organized as follows: in Sec. II we present the model independently of spatial dimensionality. In Sec. III we focus on two spatial dimensions and study the properties of the model in a quasicontinuum approach. In Sec. IV we study the effect of long-range interactions on the discrete breather excitation thresholds, and in Sec. V we corroborate our results with numerical experiments. Finally, in Sec. VI we summarize our findings and conclude.

II. MODEL AND EQUATIONS OF MOTION

We are concerned here with ILM's of the discrete nonlinear Schrödinger equation with competing short- and long-range dispersive interactions. Explicitly, we are interested in solutions of the following equation:

$$i\partial_t \psi_{\vec{n}} = -C\Delta_2 \psi_{\vec{n}} + \sum_{\vec{m}} J_{\vec{n}\vec{m}} \psi_{\vec{m}} - |\psi_{\vec{n}}|^2 \psi_{\vec{n}}, \qquad (1)$$

where $\psi_{\vec{n}}$ is the complex amplitude, $\vec{n}=(n,m)$ $(n,m=0, \pm 1, \pm 2, \ldots)$ is the lattice vector, and ∂_t denotes the time derivative. The first term in the right-hand side (rhs) of Eq. (1), with $\Delta_2 \psi_{\vec{n}} = \psi_{n,m+1} + \psi_{n,m-1} + \psi_{n+1,m} + \psi_{n-1,m} - 4\psi_{n,m}$ being the second order difference operator in two spatial dimensions, represents the short-range dispersive interaction, the second term represents the long-range dispersive interaction ($J_{\vec{n}\vec{m}}$ is the matrix element of excitation

*Permanent address: Bogolyubov Institute for Theoretical Physics, 252 143 Kiev, Ukraine.

transfer from the site $\vec{n}$ to the site $\vec{m}$), and the third term gives the nonlinearity of the excitations.

As an example of the physical system whose dynamics is governed by Eq. (1), let us consider a system of two linearly coupled excitations a and b with the excitation wave functions $a_{\vec{n}}(t)$ and $b_{\vec{n}}(t)$, respectively. The Hamiltonian of the system is

$$H = H_a + H_b + H_{ab}, \tag{2}$$

where

$$H_a = \sum_{\vec{n}} \omega_a |a_{\vec{n}}|^2 + J_a \sum_{\vec{n},\vec{\delta}} |a_{\vec{n}+\vec{\delta}} - a_{\vec{n}}|^2 - \frac{1}{2} V \sum_{\vec{n}} |a_{\vec{n}}|^4 \tag{3}$$

is the Hamiltonian of the a excitations,

$$H_b = \sum_{\vec{n}} \omega_b |b_{\vec{n}}|^2 + J_b \sum_{\vec{n},\vec{\delta}} |b_{\vec{n}+\vec{\delta}} - b_{\vec{n}}|^2 \tag{4}$$

is the Hamiltonian of the b excitations, and

$$H_{ab} = \sum_{\vec{n},\vec{\delta}} L_{\vec{n}\vec{m}} (a^*_{\vec{m}} b_{\vec{n}} + \text{c.c.}) \tag{5}$$

is the Hamiltonian of their interaction. In Eqs. (2)–(5) ω_j is the frequency of the jth ($j=a,b$) excitation, J_j is the matrix element of the j-excitation transfer (δ is the vector which connects the nearest neighbors in the lattice), V is the nonlinearity parameter, and $L_{\vec{n}\,\vec{m}}$ is the coupling between the two excitations. The matrix element $L_{\vec{n}\,\vec{m}}$ with $\vec{n}=\vec{m}$ describes an on-site coupling, while in the case $\vec{n}\neq\vec{m}$ it describes an intersite coupling of the excitations. As is seen from Eqs. (2)–(5), we assume that only the a-type of excitations are characterized by nonlinearity while the b excitations are linear. It is worth noting that the physical systems which can be modeled by a Hamiltonian like Eqs. (2)–(5) are abundant. Examples include magnon-phonon waves in ferromagnets and antiferromagnets [29,30] and magnon-libron waves in molecular antiferromagnets [30,31] [with the a excitations being the magnon complex wave amplitude and the b excitations being the phonon (libron) wave function], exciton-photon waves (polaritons) in semiconductors and molecular crystals [27], Fermi-coupled vibrational modes in molecular systems [32,33], and vibrational dynamics in superlattice structures of alternating a and b molecules [34]. Other possibilities include a coupling between acoustic and optical phonons as well as a coupling of interchain and intrachain phonon modes in nonlinear chains.

From the Hamiltonian equations (2)–(5) we obtain the equation of motion

$$i\partial_t a_{\vec{n}} = \frac{\partial H}{\partial a^*_{\vec{n}}} \qquad i\partial_t b_{\vec{n}} = \frac{\partial H}{\partial b^*_{\vec{n}}}, \tag{6}$$

for the wave functions $a_{\vec{n}}$ and $b_{\vec{n}}$ in the form

$$i\partial_t a_{\vec{n}} = \omega_a a_{\vec{n}} - J_a \Delta_2 a_{\vec{n}} + \sum_{\vec{m}} L_{\vec{n}\vec{m}} b_{\vec{m}} - V|a_{\vec{n}}|^2 a_{\vec{n}}, \tag{7}$$

$$i\partial_t b_{\vec{n}} = \omega_b b_{\vec{n}} - J_b \Delta_2 b_{\vec{n}} + \sum_{\vec{m}} L_{\vec{n}\vec{m}} a_{\vec{m}}. \tag{8}$$

From these equations, through the derivation given in the Appendix, we obtain Eq. (1) with a long-range kernel $J_{\vec{m}\vec{n}}$ given by Eq. (A15) of the Appendix. It can thus be seen that the dynamics of two linearly coupled excitations, one of which is linear and another is nonlinear, may be reduced to a single nonlinear Schrödinger equation with short- and long-range dispersive interactions. The latter describes an interaction mediated by the linear excitation. Note that Eq. (1) may be obtained from the Hamiltonian

$$\mathcal{H} = \frac{C}{2} \sum_{\vec{n}\vec{\delta}} |\psi_{\vec{n}+\vec{\delta}} - \psi_{\vec{n}}|^2 + \sum_{\vec{n}\vec{m}} J_{\vec{n}\vec{m}} \psi^*_{\vec{n}} \psi_{\vec{m}} - \frac{1}{2} \sum_{\vec{n}} |\psi_{\vec{n}}|^4, \tag{9}$$

which, together with the number of excitations (or the "power")

$$P = \sum_{\vec{n}} |\psi_{\vec{n}}|^2, \tag{10}$$

are conserved quantities.

III. QUASICONTINUUM APPROACH

In the quasicontinuum approach, regarding $\vec{n}$ as a continuum variable: $\vec{n}\to\vec{r}$, $\psi_{\vec{n}}(t)\to\psi(\vec{r},t)$, Eq. (1) with $J_{\vec{n}\vec{m}}$ given by Eq. (A15) can be written as a pseudodifferential equation

$$i\partial_t \psi = \frac{2\pi F}{\alpha^2}\psi - \left(C - \frac{2\pi F}{\alpha^2} \frac{1}{\alpha^2 - \nabla^2} \right) \nabla^2 \psi - |\psi|^2 \psi, \tag{11}$$

where ∇^2 is the two-dimensional Laplacian operator and C, α, F are given by Eqs. (A10), (A11), (A12). It is seen from Eq. (11) that for weak long-range interactions such that

$$F < F_{cr} \equiv \frac{C\alpha^4}{2\pi}, \tag{12}$$

the linear part of Eq. (11) represents the dispersion with a positive effective mass. In this case one can expect that the properties of continuumlike (i.e., wide) nonlinear excitations should be the same as in the case of the usual two-dimensional NLS equation

$$i\partial_t \psi - \nabla^2 \psi - |\psi|^2 \psi = 0. \tag{13}$$

It is known for Eq. (13) (see, for example, [35]) that the stable stationary solutions

$$\psi(\vec{r},t) = e^{i\Lambda t}\phi(\vec{r}) \tag{14}$$

with a real shape function $\phi(\vec{r})$ and a frequency Λ to Eq. (13) exist only for

$$P \equiv \int d\vec{r} |\psi(\vec{r})|^2 = P_{cr} \approx 11.7. \tag{15}$$

For $P < P_{cr}$ the excitations disperse while for $P > P_{cr}$ they collapse. On the basis of these results, we can immediately conclude that in the case of competing short- and long-range dispersions the critical power for which the stationary solutions to Eq. (11) exist is given by

$$P_{cr} = 11.7\left(C - \frac{2\pi F}{\alpha^4} \right). \tag{16}$$

For $F = F_{cr}$, P_{cr} vanishes and ILM's exist for an arbitrarily small power (as in the case of the one-dimensional NLS equation). The reason for this is as follows. $F = F_{cr}$ is a transition point: in the limit of small gradients $|\nabla\psi/\psi| \ll 1$, Eq. (11) takes the form

$$i\partial_t \psi = \frac{2\pi F}{\alpha^2}\psi + \frac{C}{\alpha^2}\nabla^4\psi - |\psi|^2\psi. \tag{17}$$

Introducing the ansatz (14) into this equation we obtain

$$-\Lambda\phi = \frac{2\pi F}{\alpha^2}\phi + \frac{C}{\alpha^2}\nabla^4\phi - \phi^3. \tag{18}$$

Equation (18) can be considered as an Euler-Lagrange equation for the rescaled dimensionless functional

$$\mathcal{F} = \frac{1}{2}\int \left\{ (\nabla^2\phi)^2 - \frac{1}{2}\phi^4 \right\} d\vec{r}. \tag{19}$$

The stability of the stationary solutions to Eq. (17) may be established in a way similar to that for Derrick's theorem (see, e.g., the review paper [35]). We assume that the function $\Phi(|\vec{r}|)$ is a stationary solution of Eq. (17) and in this way provides an extremum of the functional $\mathcal{F}$. It is seen from Eq. (19) that

$$2T = U, \tag{20}$$

where

$$T = \frac{1}{2}\int (\nabla^2\Phi)^2 d\vec{r}, \tag{21}$$

$$U = \frac{1}{4}\int \Phi^4 d\vec{r}. \tag{22}$$

By using the function

$$\phi = \kappa\Phi(\kappa|\vec{r}|), \tag{23}$$

where κ is a scaling parameter, and introducing it in the functional (19), we get

$$\mathcal{F} = \left(\frac{1}{2}\kappa^4 - \kappa^2 \right) U, \tag{24}$$

where Eq. (20) was used. It is seen from Eq. (24) that the function $\Phi(|\vec{r}|)$ provides a minimum of the functional (19) and the stationary solution is stable.

In the case of $F > F_{cr}$ it is convenient to present Eq. (11) in the form

$$i\partial_t \psi = \frac{2\pi F}{\alpha^2}\psi + \frac{C}{\alpha^2}\frac{k_{st}^2 + \nabla^2}{\alpha^2 - \nabla^2}\nabla^2\psi - |\psi|^2\psi, \tag{25}$$

where

$$k_{st}^2 = \alpha^2\left(\frac{F}{F_{cr}} - 1 \right). \tag{26}$$

It is seen from Eq. (25) that for $F > F_{cr}$ one can expect the existence of staggered continuum-like stationary solutions of the form

$$\psi(\vec{r},t) = e^{i\vec{k_{st}}\cdot\vec{r}} e^{i\Lambda t}\phi(\vec{r}). \tag{27}$$

IV. EXCITATION THRESHOLDS

It has been recently shown [23,36] for general nonlinearities of exponent $2\sigma+2$ in the nonlinear term of the Hamiltonian in Eq. (9) that, when the problem is considered in d spatial dimensions, there is an excitation threshold P_{th}; that is, for $P < P_{th}$, no localized discrete breather solutions can be sustained. The appearance of such a threshold occurs for $\sigma \geqslant 2/d$ as argued on the basis of scaling in [23] and rigorously proved in [36].

In view of this result, in $1+1$ dimensions such thresholds do not appear for the *cubic* nonlinearity, but they do appear in the case of $2+1$ dimensions (the marginal case of the inequality mentioned above). Such thresholds have been numerically studied in [24,25] and will also be relevant to the numerical results presented in the following section. However, they have not been discussed in the presence of competing short-range and long-range dispersive interactions. Hence, in this section we generalize the discussion of Weinstein given in [36] to include the presence of a long-range kernel, which we will symbolize by **K**. As there is no reason for a restriction to the cubic case, we will keep our discussion as general as possible, considering a nonlinearity exponent $2\sigma+2$ in the Hamiltonian. Clearly, the case of $\sigma = 1$ will be relevant to the cubic nonlinearity numerical results of the following section.

Following [36] [in particular Eq. (2.1) of that paper], the Hamiltonian can be rewritten in our case as

$$\mathcal{H} = -C(\Delta_2\psi_{\vec{n}}, \psi_{\vec{n}}) - \frac{1}{\sigma+1}\sum_{\vec{n}} |\psi_{\vec{n}}|^{2\sigma+2} + (\psi_{\vec{n}}, \mathbf{K}\cdot\psi_{\vec{m}}). \tag{28}$$

The symbolism (,) has been used for an inner product, while for the rest of this section we will suppress the subscript $\vec{n}$, denoting $\psi \equiv \psi_n^-$ for notational simplicity.

We define $I_P = \inf\{\mathcal{H}[\phi]: P[\phi] = P\}$, the infimum of the energy functional for a fixed norm. $I_\nu \geqslant 0$, for norm less than a threshold power, is needed for an excitation threshold to exist as shown in [36]. However, the latter is equivalent to the inequality

$$\frac{1}{\sigma+1} \sum |\psi|^{2\sigma+2} \leqslant C(-\Delta_2 \psi, \psi) + (\psi, \mathbf{K} \cdot \psi). \quad (29)$$

If we now rescale ψ according to

$$\psi = \sqrt{P} ||v||_2^{-1} v \quad (30)$$

(where the subscript denotes the L^2 norm of v) the inequality (29) becomes

$$\sum |v|^{2\sigma+2} \leqslant (\sigma+1) P^{-\sigma} ||v||_2^{2\sigma} [C(-\Delta_2 v, v) + (v, \mathbf{K} \cdot v)]. \quad (31)$$

Hence, when there exists a constant $C^\star$, such that

$$\sum |v|^{2\sigma+2} \leqslant C^\star ||v||_2^{2\sigma} [C(-\Delta_2 v, v) + (v, \mathbf{K} \cdot v)], \quad (32)$$

then there exists a threshold power P_{th}, satisfying $P_{th}^{-\sigma}(\sigma+1) = C^\star$, below which, according to theorems 2.1 and 3.1 of [36], no discrete breathers can be present.

From Eq. (32),

$$\frac{1}{C^\star} = J_{C,\mathbf{K}}^{\sigma,d} \equiv \inf \left[\|v\|_2^{2\sigma} \frac{C(-\Delta_2 v, v) + (v, \mathbf{K} \cdot v)}{\sum |v|^{2\sigma+2}} \right], \quad (33)$$

and it will then be true that

$$P_{th} = [(\sigma+1) J_{C,\mathbf{K}}^{\sigma,d}]^{1/\sigma}. \quad (34)$$

Now, notice that using the discrete version of the Sobolev-Nirenberg-Gagliardo (SNG) estimate by adapting Eq. (4.17) of [36], we have

$$||v||_2^{2\sigma} \frac{(-\Delta_2 v, v)}{\sum |v|^{2\sigma+2}} \geqslant \frac{1}{C_1}, \quad (35)$$

where C_1 is a constant. We can also, however, use the Schwarz inequality to bound the second term in the fractional part of Eq. (33) from below. In particular, since $\Sigma |v|^{2\sigma+2} \leqslant ||v||_2^{2\sigma+2}$, we have

$$\frac{||v||_2^{2\sigma}}{\sum |v|^{2\sigma+2}} (v, \mathbf{K} \cdot v) \geqslant (v_1, \mathbf{K} \cdot v_1), \quad (36)$$

where $v_1 = v/||v||_2$ is a vector of unit norm. Some remarks are in order.

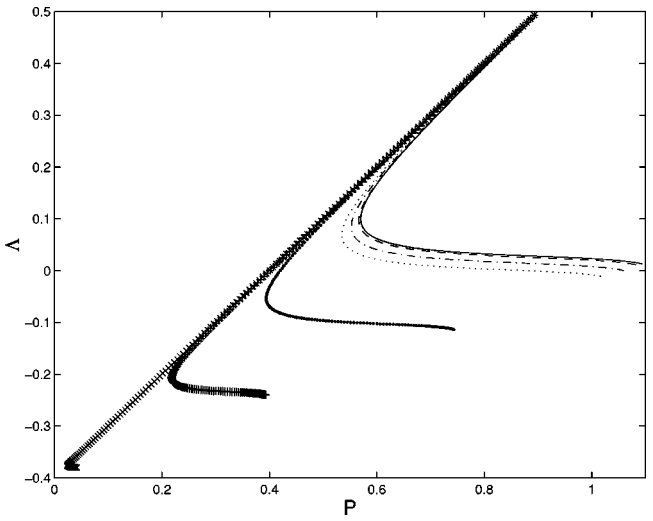

FIG. 1. Frequency of the breather solution as a function of its power is shown for various branches of subcritical long-range interaction amplitude F. The solid line shows the branch for $F=0$; this is the same (stable) branch shown in [25,26] where only short-range interactions were considered. The dashed line shows the branch for $F=1$; the dash-dotted for $F=5$; the dotted for $F=10$; the points for $F=50$; the plus symbols (next to last branch) for $F=100$; and finally the x symbols (the leftmost branch) for $F=162$ very close to the critical point. The parameters used are detailed in the text. Notice that the upper branch (above the turning point) is always stable, while the lower is always unstable (see also the relevant remarks in the text). $C=0.1$, $\alpha=3$.

(i) Since the quantity $(v_1, K \cdot v_1)$ is positive definite, for small (positive) F (amplitude of the long-range interaction), there will still be an excitation threshold. In fact, the right-hand side of Eq. (33) will still be $\geqslant 1/C_1$ (the infimum obtained for the case with short-range interactions only) and hence, an excitation threshold will be present.

(ii) To understand the dependence of the threshold value on F, we compare the cases of two different values F_1, F_2, with $F_2 > F_1 > 0$. In the case of F_2, since the second term in the quotient is positive definite, a smaller norm excitation (than in the case of F_1) is needed to obtain the same value of the quotient. Hence the threshold for excitation of the intrinsic localized modes will be decreased; in fact, due to the linear dependence of P_{th} on $J_{C,\mathbf{K}}^{\sigma,d}$ (in the cubic case) and of $J_{C,\mathbf{K}}^{\sigma,d}$ on F (in general), the excitation threshold should be expected to decrease linearly with F. An alternative way to understand this result is by observing the competing nature of the dispersive terms in the context of Eq. (11). Similar considerations in the case of $F<0$ yield the prediction of a linear increase in P_{th}.

V. NUMERICAL RESULTS

We now turn to a numerical investigation of Eq. (1) in $2+1$ dimensions. In particular, we look for standing wave solutions of the form of Eq. (14). Equation (1) then becomes

$$G(\Lambda, \phi_n^-) \equiv \Lambda \phi_n^- C \Delta_2 \phi_n^- + F \sum_{\vec{m} \neq \vec{n}} K_0(\alpha |\vec{m} - \vec{n}|) \phi_m^- |\phi_n^-|^2 \phi_n^- = 0. \quad (37)$$

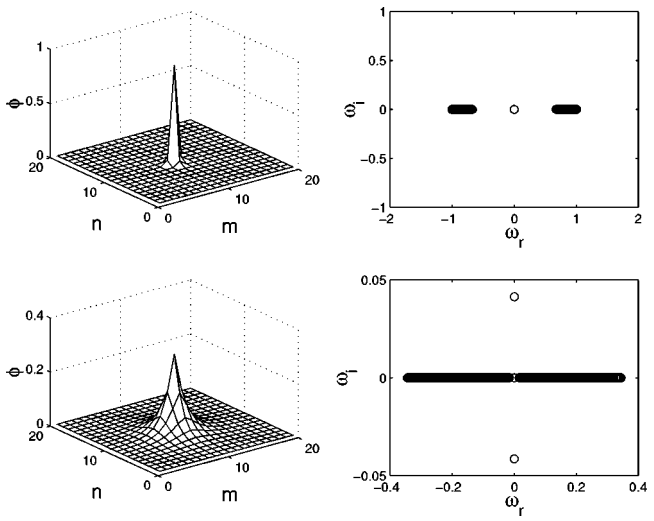

FIG. 2. Typical profile of behavior on the stable (upper) and unstable (lower) portion of a branch. The results are for $F=100$. A typical stable solution is shown in the top left panel for $\Lambda=0.43$, $P=0.83$. The top right panel shows the results of linear stability analysis and the real values of ω indicate stability. The bottom left panel shows the unstable solution obtained for $\Lambda=-0.232$, $P=0.28$ below the turning point. The linear stability analysis in the bottom right panel indicates, as emphasized in the text, the presence of an unstable eigenmode. $C=0.1$, $\alpha=3$.

We use the methods of [24] to solve Eq. (37) and the continuation methods of [25] to obtain a branch of solutions.

Once the solution is found, linear stability analysis is performed around the solution. In particular, a solution of the form $\psi_{\vec{m}}=\exp(i\Lambda t)(\phi_{\vec{m}}+\epsilon u_{\vec{m}})$ is considered and $u_{\vec{n}}$ is analyzed as $u_{\vec{n}}=v_{\vec{n}}\exp(-i\omega t)+w_{\vec{n}}\exp(i\omega^{\star}t)$, resulting in an eigenvalue problem for $\{\omega,\{v_{\vec{n}},w_{\vec{n}}\}\}$.

Solving numerically Eq. (37) and the eigenvalue problem for $\{\omega,\{v_{\vec{n}},w_{\vec{n}}\}\}$, we obtain the different branches of Fig. 1. C is fixed to 0.1. In Fig. 1, α is also fixed to $\alpha=3$ which should be rescaled by the lattice spacing h $(=\sqrt{1/C})$ in view of Eq. (37). The rescaling yields an "effective" $\alpha_{\rm eff}=3h\approx 9.487$ which should be used in the equations of the quasicontinuum approach of Sec. III [e.g., Eqs. (12) and (16)]. We conclude from Fig. 1 that, as the amplitude of the long-range interaction is increased, the threshold power needed for the generation of the excitation is suppressed, as discussed in Sec. IV. Below the turning point of the branch, unstable solutions are obtained. This conclusion is in agreement with the studies of [24,25] as well as with the theory of [37]. The latter predicts that unstable configurations arise when $dP/d\Lambda<0$. The typical instability scenario (see Fig. 2) involves the bifurcation of a pair of eigenvalues from the continuous spectrum and its eventual passing through the origin and becoming imaginary.

Comparing the different branches, we arrive at the following conclusions.

(i) In agreement with the theory of Sec. IV, the threshold for the excitation of the discrete breathers is lowered in the presence of the long-range interaction (when $F>0$), and is eventually completely suppressed (see also below).

(ii) The width of the unstable branch decreases, in accordance with Eq. (16). In particular, as was noted in [24], this branch terminates in a tricritical point that coincides with the critical power for collapse in the continuum case, $P_{cr}\approx 11.7C$. At that point all branches degenerate to extended waves (phonons). As predicted by Eq. (16), the critical point of the branch termination is shifted. Hence, since the threshold suppression is slower than the critical power suppression, the unstable branch width decreases as F increases.

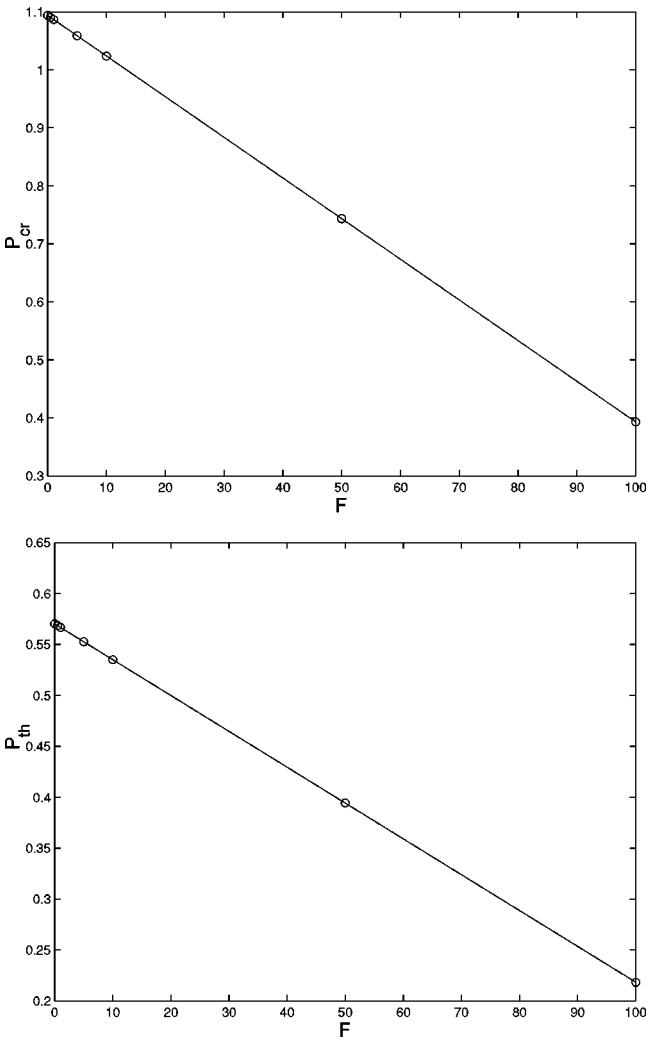

FIG. 3. Dependence of the critical power P_{cr} (top panel) and of the threshold power P_{th} (bottom panel) defined in Secs. III and IV of the text, respectively, on the amplitude F of the long-range interaction. See the text for a detailed discussion on the linear dependence as well as for the best fits given by the solid line (the individual simulation data points from each branch are marked by circles). $C=0.1$, $\alpha=3$.

(iii) The dependence of P_{cr} (for the various branches) on F is shown to be linear in the upper panel of Fig. 3. The best fit is given by $P_{cr}=-0.0075F+1.0939$ in fair agreement with the prediction of 0.0091 for the slope and 1.17 for the intercept. The discrepancy is accounted for (quite clearly in the simulations) by boundary effects. Due to the computational cost of two-dimensional numerical calculations, the branches were constructed in small domains (20×20 sites), for which the delocalization (broadening) of the discrete

pulses occurs at smaller values of the critical power. In fact, limited calculations in larger domains gave better comparison with the theoretical prediction (i.e., the slope was found to be -0.008 and the intercept 1.14 in the latter case).

(iv) For the threshold power P_{th}, a linear dependence is also found on F, in agreement with the theory of Sec. IV. The dependence on F is given by $P_{th}=-0.0035F+0.5701$. Thus P_{cr} decreases twice as fast, resulting in the eventual disappearance of the unstable branch. This dependence is shown in the lower panel of Fig. 3.

(v) We also observed the dependence of the same quantities (the branches, as well as P_{cr}, P_{th}) on α. Once again good agreement was found with the theoretical predictions for the slope of -4.

(vi) Solutions were also constructed for negative values of F. In particular, it was observed that the branch moves inwards in this case, increasing the critical as well as the threshold powers, as was theoretically predicted. The linear dependencies of P_{cr}, P_{th} on F (considered independently from the ones for $F>0$), were found to agree very well with the linear predictions obtained for $F>0$.

It should be remarked here that bistability was not observed in the branches of solutions of the two-dimensional system in agreement with the findings of [26] also for $2+1$ dimensional discrete systems. This is a feature particular to the higher (spatially) dimensional discrete systems that should be contrasted to the $1+1$ dimensional ones of [6,9].

A last question that we consider separately is what happens beyond the critical point at which the threshold disappears. The quasicontinuum methodology predicts $F_{cr}\approx 130$ for the parameters considered here. In the numerical computations $F_{cr}\approx 162.5$. Once again, the discrepancy between the two results is due to the role of the boundaries and also the significant role of the nonlinearity. Notice that the calculations of Sec. III are valid for $P\to 0$ and broad pulses. On the contrary, at the beginning of the branch P is of $O(1)$ and the solutions are very strongly localized, hence nonlinear effects should affect the specific values of where the linear phenomena should appear but not the phenomenology itself. In fact, beyond the critical point, A typical example is shown in Fig. 4 for $F=225$, where the two-dimensional profile ϕ is shown as well as (lower panel) a one-dimensional cut through the center of the breather profile. It should be noted that in the supercritical cases studied, due to the sparsity of available wave numbers in the finite and small lattices used, the discrete breathers were found to lock almost always in the wave vector $\vec{k}=(\pi,\pi)$. However, as predicted in Sec. III, staggered solution branches are found beyond the critical point. It should also be noted that for some of the staggered branches, the unstable branch typically present for short-range interactions can be completely suppressed by the effect of the long-range interactions.

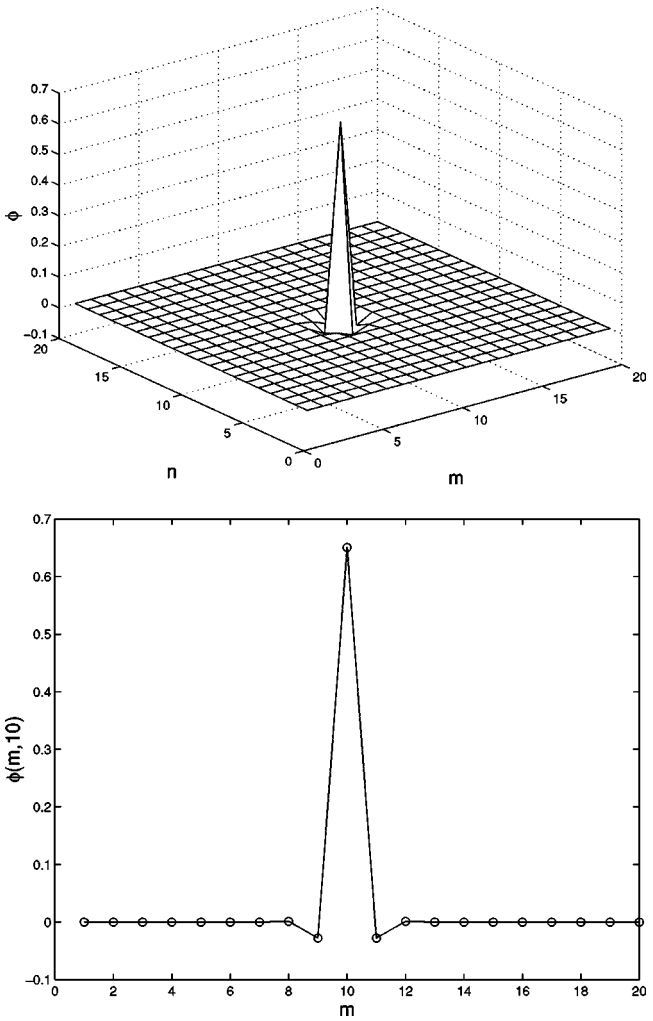

FIG. 4. Profile of a staggered solution for $F=225$, $\Lambda=0.028$, $P=0.428$. The upper panel shows the two-dimensional profile of the solution, while the lower panel shows a one-dimensional cut through the center of the solution. The staggered nature of the solution is clearly observed. $C=0.1$, $\alpha=3$.

VI. CONCLUSIONS

In this paper we studied the effects of competing short-range and long-range dispersive interactions on intrinsic localized modes (or discrete breathers) in the presence of nonlinearity. We developed a specific model relevant to situations in condensed matter physics, in particular concerning coupling of two excitations (such as, for example, phonon-magnon, phonon-libron, or exciton-phonon excitations). This model was demonstrated to be equivalent to a discrete nonlinear Schrödinger-type (DNLS) model with long-range interactions (mediated by the coupling to the second excitation).

We analyzed this DNLS equation from a quasicontinuum perspective in two spatial dimensions, and made predictions about the modification of the critical power, beyond which collapse is present in the continuum case. On the basis of this analysis, for appropriate (supercritical) values of the long-range kernel amplitude, we predicted staggered excitations.

The same DNLS model with competing short- and long-range interactions was also theoretically analyzed from a fully discrete perspective. We used appropriate norm estimates, following the methodologies of [36], to establish the presence of excitation power thresholds and their dependence on the amplitude of the long-range kernel.

Finally, we complemented these results by numerical experiments, in which branches of *exact* standing wave solutions were constructed and their linear stability was analyzed. We verified the theoretical prediction for the suppression of the critical and the threshold power, and demonstrated their linear dependence on the amplitude and power law dependence on the range of the interaction studied. Furthermore, the predicted staggered solutions for supercritical values of the long-range amplitude were also observed in the numerical results.

Our results constitute an increased understanding of the effects of competitions of different types of dispersive interactions in relevant physical systems and materials. It would clearly be desirable to generalize such considerations to the case of three-dimensional systems. This challenging task will be left for future studies.

ACKNOWLEDGMENTS

Yu. Gaididei is grateful for the hospitality of the Los Alamos National Laboratory where this work was performed. Work at Los Alamos is performed under the auspices of the U.S. Department of Energy, under Contract No. W-7405-ENG-36.

APPENDIX: DERIVATION OF EQ. (1) FROM THE COUPLED EXCITATIONS' MODEL

By applying the Fourier transforms

$$b_{\vec{k}}(t)=\frac{1}{N}\sum_{\vec{n}} e^{i\vec{k}\cdot\vec{n}}b_{\vec{n}}(t),$$

$$\overline{b_{\vec{n}}}(\omega)=\int_{-\infty}^{\infty} e^{-i\omega t}b_{\vec{n}}(t)dt, \tag{A1}$$

where N is the number of sites in the lattice, Eq. (8) can be presented in the form

$$\overline{b_{\vec{k}}}(\omega)=\frac{L(\vec{k})}{\omega-\omega_b(\vec{k})}\overline{a_{\vec{k}}}(\omega). \tag{A2}$$

Here the notation

$$\omega_j(k)=\omega_j+J_j\Delta(\vec{k}) \tag{A3}$$

for the frequency of the j excitation ($j=a,b$) is introduced,

$$\Delta(\vec{k})=\sum_{\vec{\delta}} (1-e^{i\vec{k}\cdot\vec{\delta}}), \tag{A4}$$

is the Fourier transform of the second difference operator Δ_2, and

$$L(\vec{k})=\sum_{\vec{n}} e^{i\vec{k}\cdot\vec{n}}L_{\vec{n}\vec{o}}. \tag{A5}$$

Applying the Fourier transformation in Eq. (7) and inserting Eq. (A2) into the obtained equation we get

$$\frac{[\omega-\omega_+(\vec{k})][\omega-\omega_-(\vec{k})]}{\omega-\omega_b(\vec{k})}\overline{a_{\vec{k}}}(\omega) = V\frac{1}{N}\sum_{\vec{n}}\int_{-\infty}^{\infty} e^{i\vec{k}\cdot\vec{n}-i\omega t}|a_{\vec{n}}(t)|^2a_{\vec{n}}(t), \tag{A6}$$

where

$$\omega_{\pm}(\vec{k})=\frac{1}{2}\{\omega_a(\vec{k})+\omega_b(\vec{k})\pm\sqrt{[\omega_a(\vec{k})-\omega_b(\vec{k})]^2+4L^2(\vec{k})}\} \tag{A7}$$

are the eigenfrequencies of the linear part of the Hamiltonian (2)–(5).

Let us consider the case when $\omega_a>\omega_b$ and $J_b<0$ (negative effective mass of the b excitation), and $L_{\vec{n}\vec{m}}=L\delta_{\vec{n}\vec{m}}$ (on-site coupling between a and b excitations). Being interested in the excitations that belong to the gap interval: $\omega_-(\vec{k})<\omega<\omega_+(\vec{k})$ and considering, in particular, the excitations with frequencies close to $\omega_+(\vec{k})$, we obtain instead of Eq. (A6) approximately

$$\left(\omega-\omega_0-C\Delta(\vec{k})-\frac{2\pi F}{\alpha^2+\Delta(\vec{k})}\right)\overline{a_{\vec{k}}}(\omega) = V\frac{1}{N}\sum_{\vec{n}}\int_{-\infty}^{\infty} e^{i\vec{k}\cdot\vec{n}-i\omega t}|a_{\vec{n}}(t)|^2a_{\vec{n}}(t), \tag{A8}$$

where the parameters

$$\omega_0=\frac{\omega_a+\omega_b}{2}+\frac{(\omega_a-\omega_b)^2-2L^2}{2(\omega_a-\omega_b)^2}\sqrt{(\omega_a-\omega_b)^2+4L^2}, \tag{A9}$$

$$C=\frac{J_a+J_b}{2}+\frac{J_a-J_b}{2}\frac{(\omega_a-\omega_b)^2+2L^2}{(\omega_a-\omega_b)\sqrt{(\omega_a-\omega_b)^2+4L^2}}, \tag{A10}$$

$$\alpha^2=\frac{(\omega_a-\omega_b)^2+4L^2}{(\omega_a-\omega_b)(J_a-J_b)}, \tag{A11}$$

$$2\pi F=\frac{L^2}{J_a-J_b}\left(1+\frac{4L^2}{(\omega_a-\omega_b)^2}\right)^{3/2} \tag{A12}$$

were obtained by using a Padé approximation of degree (1,1) with respect to $\Delta(\vec{k})$ [38]. Applying the inverse Fourier transform and using the gauge transform

$$a_{\vec{n}}(t)=\frac{1}{\sqrt{V}}\psi_{\vec{n}}(t)e^{-i\omega_0 t}, \tag{A13}$$

we obtain Eq. (1) with the matrix element of the long-range dispersive interaction $J_{\vec{n}\vec{m}}$ in the form

$$J_{\vec{n}\vec{m}} = 2\pi F \frac{1}{N} \sum_{\vec{k}} \frac{e^{i\vec{k}\cdot(\vec{n}-\vec{m})}}{\alpha^2 + \Delta(\vec{k})}. \tag{A14}$$

Notice that, up to this point, our presentation has been kept as general as possible and, in particular, is independent of dimensionality. From now on we restrict ourselves to two spatial dimensions. For $|\vec{n}-\vec{m}| \gg 1$ only small wave numbers $|\vec{k}| \ll 1$ contribute significantly to the integral (A14) and one can obtain that

$$J_{\vec{n}\vec{m}} \approx 2\pi F \frac{1}{(2\pi)^2} \int \frac{e^{i\vec{k}\cdot(\vec{n}-\vec{m})}}{\alpha^2 + \vec{k}^2} d\vec{k} = F K_0(\alpha|\vec{n}-\vec{m}|), \tag{A15}$$

where $K_0(x)$ is the Bessel function of the second order [39]. The parameter C given by Eq. (A10) represents an effective short-range dispersion, while the parameters α and F from Eqs. (A11) and (A12) give the inverse radius of the long-range interaction and its intensity, respectively. In the body of the paper, the matrix element of the long-range excitation transfer $J_{\vec{n}\vec{m}}$ has been used in the form (A15).

[1] R. Lai and A.J. Sievers, Phys. Rep. **314**, 148 (1999).
[2] A.S. Davydov, *Solitons in Molecular Systems* (Reidel, Dordrecht, 1985).
[3] A.C. Scott, Phys. Rep. **217**, 1 (1996).
[4] M. Peyrard and A.R. Bishop, Phys. Rev. Lett. **62**, 2755 (1989); T. Dauxois, M. Peyrard, and A.R. Bishop, Phys. Rev. E **47**, 684 (1993).
[5] L.V. Yakushevich, *Nonlinear Physics of DNA* (Wiley, New York, 1998).
[6] Yu. B. Gaididei, S. F. Mingaleev, P.L. Christiansen, M. Johansson, and K.Ø. Rasmussen, in *Nonlinear Cooperative Phenomena in Biological Systems*, edited by L. Mattson (World Scientific, Singapore, 1998), p. 176.
[7] *Photonic Band Gaps and Localization*, edited by C.M. Soukoulis (Plenum, New York, 1993); *Photonic Band Gap Materials*, edited by C.M. Soukoulis (Kluwer, London, 1996).
[8] D. Hennig and G.P. Tsironis, Phys. Rep. **307**, 334 (1999).
[9] Yu.B. Gaididei, P.L. Christiansen, K.Ø. Rasmussen, and M. Johansson, Phys. Rev. B **55**, R13365 (1997).
[10] C.B. Clausen, P.L. Christiansen, L. Torner, and Yu.B. Gaididei, Phys. Rev. E **60**, R5064 (1999).
[11] A.R. McGurn, Phys. Lett. A **251**, 322 (1999); **260**, 314 (1999).
[12] S.F. Mingaleev, Yu.S. Kivshar, and R.A. Sammut, Phys. Rev. E **62**, 5777 (2000).
[13] S. Flach and C.R. Willis, Phys. Rep. **295**, 181 (1995).
[14] Special issue on *Future Directions of Nonlinear Dynamics in Physical and Biological Systems*, edited by P.L. Christiansen, J.C. Eilbeck, and R.D. Parmentier [Physica D **68** (1993)].
[15] B.I. Swanson, J.A. Brozik, S.P. Love, G.F. Strouse, A.P. Shreve, A.R. Bishop, W.Z. Wang, and M.I. Salkola, Phys. Rev. Lett. **82**, 3288 (1999).
[16] R.S. MacKay and S. Aubry, Nonlinearity **7**, 1623 (1994).
[17] F. Fisher, Ann. Phys. (Leipzig) **2**, 296 (1993).
[18] S. Flach, K. Kladko, and S. Takeno, Phys. Rev. Lett. **79**, 4838 (1997).
[19] V.M. Burlakov, S.A. Kiselev, and V.N. Pyrkov, Phys. Rev. B **42**, 4921 (1990).
[20] S. Flach, K. Kladko, and C.R. Willis, Phys. Rev. E **50**, 2293 (1994).
[21] J.M. Tamga, M. Remoissenet, and J. Pouget, Phys. Rev. Lett. **75**, 357 (1995).
[22] J. Pouget, M. Remoissenet, and J.M. Tamga, Phys. Rev. B **47**, 14 866 (1993).
[23] S. Flach, K. Kladko, and R.S. MacKay, Phys. Rev. Lett. **78**, 1207 (1997).
[24] P.G. Kevrekidis, K.Ø. Rasmussen, and A.R. Bishop, Phys. Rev. E **61**, 2006 (2000); **61**, 4652 (2000).
[25] P.G. Kevrekidis, K.Ø. Rasmussen, and A.R. Bishop, Math. Comput. Simul. **55**, 449 (2001).
[26] P.L. Christiansen, Yu.B. Gaididei, M. Johansson, K.Ø. Rasmussen, V.K. Mezentsev, and J.J. Rasmussen, Phys. Rev. B **57**, 11 303 (1998).
[27] A.S. Davydov, *Theory of Molecular Excitons* (Nauka, Moscow, 1967).
[28] D. Möbius, Adv. Mater. **7**, 437 (1995).
[29] A.I. Akhiezer, V.G. Baryakhtar, and S.V. Peletrminskii, *Spin Waves* (Nauka, Moscow, 1967; North-Holland, Amsterdam, 1968).
[30] Yu.B. Gaididei, V.M. Loktev, and V.S. Ostrovsky, Fiz. Nizk. Temp. **11**, 740 (1985) [Sov. J. Low Temp. Phys. **11**, 406 (1985).
[31] Yu.B. Gaididei, V.M. Loktev, V.S. Ostrovsky, and A.F. Prikhotko, Fiz. Nizk. Temp. **12**, 61 (1986) [Sov. J. Low Temp. Phys. **12**, 36 (1986).
[32] G. Herzberg, *Molecular Spectra and Molecular Structure. II. Infrared and Raman Spectra of Polyatomic Molecules* (Van Nostrand, New York, 1959).
[33] N. Levin, *Molecular Spectroscopy* (Wiley, New York, 1975).
[34] V.M. Agranovich, O.A. Dubovsky, and A.M. Kamchatnov, Chem. Phys. **198**, 245 (1995).
[35] J.J. Rasmussen and K. Rypdal, Phys. Scr. **33**, 481 (1986).
[36] M. Weinstein, Nonlinearity **12**, 673 (1999).
[37] M.G. Vakhitov and A.A. Kolokolov, Sov. Radiophys. **16**, 783 (1973).
[38] *Padé Approximants Method and its Applications to Mechanics*, edited by H. Cabannes (Springer-Verlag, Berlin, 1976); G. A. Baker, Jr. and P. Graves-Morris, *Padé Approximants*, Encyclopedia of Mathematics and its Applications Vol. 59 (Cambridge University Press, Cambridge, 1996).
[39] *Handbook of Mathematical Functions*, edited by M. Abramowitz and I. Stegun (Dover, New York, 1972).